Appendix I

Finite Element Analysis (FEA)

A.1.1. FEA

Finite element analysis (FEA) is a computational technique widely used to estimate the behavior of structures under loading. Briefly, the technique uses a series of small elements that can be a variety of shapes, and that are connected at nodal points. The elements can be assigned properties that are indicative of the tissue properties that small areas of the biological structure have, either relying on measurements that have been made of the properties of the material, or in those cases in which the properties have not been measured, estimating them based on what we do know. For most models, properties for elastic modulus (tissue stiffness) are assigned to the entire structure, which can be a poor representation of bone tissue properties given one's heterogeneity, rather than to individual elements. A virtual load can be applied to this structure, and the displacement (or deformation) of the structure under that loading condition can be estimated. A second method, known as the flexibility method, is based on known displacements. Knowing the load and the displacement, it is possible to calculate the stresses and strains within the structure, which can provide valuable information to estimate how the structure will "perform" mechanically.

FEA does not prove that something is true, but only suggests what might happen under certain idealized circumstances, assuming that the circumstances one has entered into the computation are correct (or at least within a reasonable margin of error). Therefore, it is important that the conditions of the model could be verified, that the results could be somehow validated, and that the sensitivity of the model to variations in the input parameters could be assessed. Although FEA has been used successfully for many years, any new FEA model chooses specific parameters for bone material properties, and determines specific "boundary conditions" under which the model will operate. These will vary for each new FEA model, and; therefore, each new model must be validated. [Burr, 2016]

A.1.2. High resolution FEM

High resolution finite element models derived from micro-computed tomography images are often used to study the effects of trabecular microarchitecture

and loading mode on tissue stress, but the degree to which existing finite element methods correctly predict the location of tissue failure is not well characterized. But also high resolution finite element models, derived from three dimensional images of trabecular bone microstructure, are the primary means of estimating tissue level stress and strain in cancellous bone. Modern high-resolution finite element models of cancellous bone are capable of predicting apparent yield strength and are often used to estimate the amount of tissue damage generated by overloads [Goff et al., 2015].

To date, finite element modelling of trabecular bone failure has in general been limited to damage mechanisms alone. Computationally, this process is somewhat straightforward to represent. Typically, the mechanical properties of the damaged elements are modified to represent the tissue of lower stiffness. This approach has previously been successfully implemented in high-resolution image-based (voxel) finite element analysis software to accurately determine the tissue damage strains and the 'macro'-level (bulk specimen with multiple trabecular struts) yield point.

However, it has been reported that the square-based mesh structures have been found suitable for fracture modelling as it allows cracks to follow straight paths if so desired, or deviate in stepped lines around element boundaries, and is also preferable to irregular meshes for mixed-mode fracture. Harrison et al. aimed to utilise 3D voxel (only regular 3D solid hexahedral elements, all with the same shape, size and orientation) meshes for cohesive modelling of trabecular bone without placing traditional cohesive elements between every two 3D solid elements from the start of the simulation. [Harrison et al., 2013]

Digital finite element (FE) models, composed mostly of a mesh of eight-node brick elements created directly from CT voxels or after resampling, are potentially useful for evaluating the effects of bone diseases and their subsequent treatments on the mechanical properties of trabecular bone. The reliability and accuracy of such models to predict mechanical properties relies on many factors. [Chevalier et al., 2007]

Despite the high clinical relevance of trabecular bone fractures, there is still a need to develop validated micro-CT FE models describing the complete fracture behavior of trabecular bone specimens in a simple way. A quantitative assessment of trabecular level conditions associated with initiation of microdamage until total fracture may provide insight into the improvement of fracture risk assessment methods and the development of therapeutic strategies for the treatment of skeletal fragility diseases such as osteoporosis. [Hambli, 2013]

A.1.3. Element types considered for the FEA

a. Linear tetrahedral elements (C3D4)

The C3D4 is a general purpose tetrahedral element (1 integration point). The node numbering follows the convention of *Figure 1*.

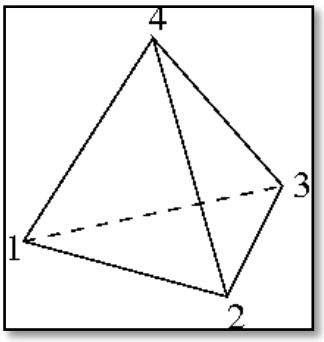

Figure 1: *Linear tetrahedral element*

This element is included for completeness, however, it is not suited for structural calculations unless a lot of them are used (the element is too stiff).

b. Quadratic tetrahedral elements (C3D10)

The C3D10 element is a general purpose tetrahedral element (4 integration points). The node numbering follows the convention of *Figure 2*.

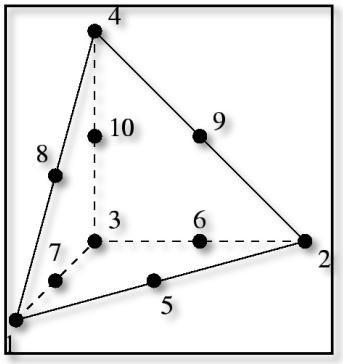

Figure 2: *Quadratic tetrahedral element*

The element behaves very well and is a good general purpose element. The C3D10 element is especially attractive because of the existence of fully automatic tetrahedral meshers.

c. Voxel (C3D8)

The C3D8 element is a general purpose linear brick element, fully integrated (2x2x2 integration points). The node numbering follows the convention of *Figure 3* and the integration points are numbered according to *Figure 4*.

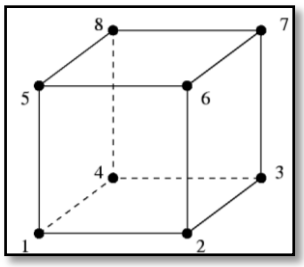

Figure 3: *Voxel element*

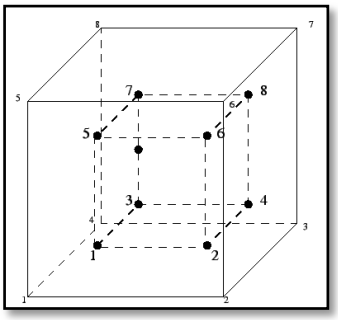

Figure 4: *2x2x2 integration point scheme in hexahedral elements*

Although the structure of the element is straightforward, it should not be used in the following situations:

- Due to the full integration, the element will behave badly for isochoric material behavior, i.e. for high values of Poisson's coefficient or plastic behavior.
- The element tends to be too stiff in bending, e.g. for slender beams or thin plates under bending.

Appendix II

Mesh characteristics

As regards the finite element analyses of all specimens, the resulting FE models were imported into the commercial FE software package ABAQUS (Dassault Systèmes Simulia Corp., Suresnes Frances). In following tables it can be observed the mesh characterisitics for each specimen.

Specimen 15_8	Linear tetrahedral mesh	Quadratic tetrahedral mesh	Voxel mesh
N Elements	81954	81954	53742
N Nodes	29735	169754	88417

Specimen 15_9	Linear tetrahedral mesh	Quadratic tetrahedral mesh	Voxel mesh
N Elements	74431	74431	42242
N Nodes	27417	155689	72779

Specimen 15_10	Linear tetrahedral mesh	Quadratic tetrahedral mesh	Voxel mesh
N Elements	33775	33775	40842
N Nodes	13729	74832	70136

Specimen 15_11	Linear tetrahedral mesh	Quadratic tetrahedral mesh	Voxel mesh
N Elements	46305	46305	69298
N Nodes	17768	99176	108292

Specimen 15_12	Linear tetrahedral mesh	Quadratic tetrahedral mesh	Voxel mesh
N Elements	113336	113336	65742
N Nodes	38758	227124	104244

Specimen 15_13	Linear tetrahedral mesh	Quadratic tetrahedral mesh	Voxel mesh
N Elements	52543	52543	84008
N Nodes	19586	110845	128929

Specimen 20_8	Linear tetrahedral mesh	Quadratic tetrahedral mesh	Voxel mesh
N Elements	16464	16464	43956
N Nodes	6422	35691	67179

Specimen 20_9	Linear tetrahedral mesh	Quadratic tetrahedral mesh	Voxel mesh
N Elements	66204	66204	67938
N Nodes	22523	132404	100394

Specimen 20_10	Linear tetrahedral mesh	Quadratic tetrahedral mesh	Voxel mesh
N Elements	44295	44295	124814
N Nodes	16221	92689	182328

Specimen 20_11	Linear tetrahedral mesh	Quadratic tetrahedral mesh	Voxel mesh
N Elements	105407	105407	72592
N Nodes	33049	201138	106069

Specimen 20_12	Linear tetrahedral mesh	Quadratic tetrahedral mesh	Voxel mesh
N Elements	88744	88744	68082
N Nodes	28957	173012	101894

Specimen 20_13	Linear tetrahedral mesh	Quadratic tetrahedral mesh	Voxel mesh
N Elements	102184	102184	72214
N Nodes	33561	200401	106923

Specimen 30_5	Linear tetrahedral mesh	Quadratic tetrahedral mesh	Voxel mesh
N Elements	35266	35266	123740
N Nodes	13346	75493	181042

Specimen 30_9	Linear tetrahedral mesh	Quadratic tetrahedral mesh	Voxel mesh
N Elements	96558	96558	96702
N Nodes	33394	194882	144132

Specimen 30_10	Linear tetrahedral mesh	Quadratic tetrahedral mesh	Voxel mesh
N Elements	67439	67439	58468
N Nodes	23798	137463	89608

Specimen 30_14	Linear tetrahedral mesh	Quadratic tetrahedral mesh	Voxel mesh
N Elements	100796	100796	88559
N Nodes	33443	198706	129263

Specimen 30_15	Linear tetrahedral mesh	Quadratic tetrahedral mesh	Voxel mesh
N Elements	38185	38185	89267
N Nodes	13676	78568	125119

Specimen 30_16	Linear tetrahedral mesh	Quadratic tetrahedral mesh	Voxel mesh
N Elements	126241	126241	83999
N Nodes	40759	244784	122735

Appendix III

Detailed experimental results

Although all tested specimens were submitted to a quality control to ensure specimens´ homogeneity, it should be pointed out that in some cases Young´s Modulus increases its value significantly, because the progressive contact of trabeculae generates the compaction of the specimen microstructure. Furthermore, it is observed that the last seven specimens of each porosity showed better results that the first seven because of the better quality control carried out, in which better machining specimens were chosen.

Some specimens have *, because those specimens were scanned using a microcomputed tomography system and later they were simulated using the FE method.

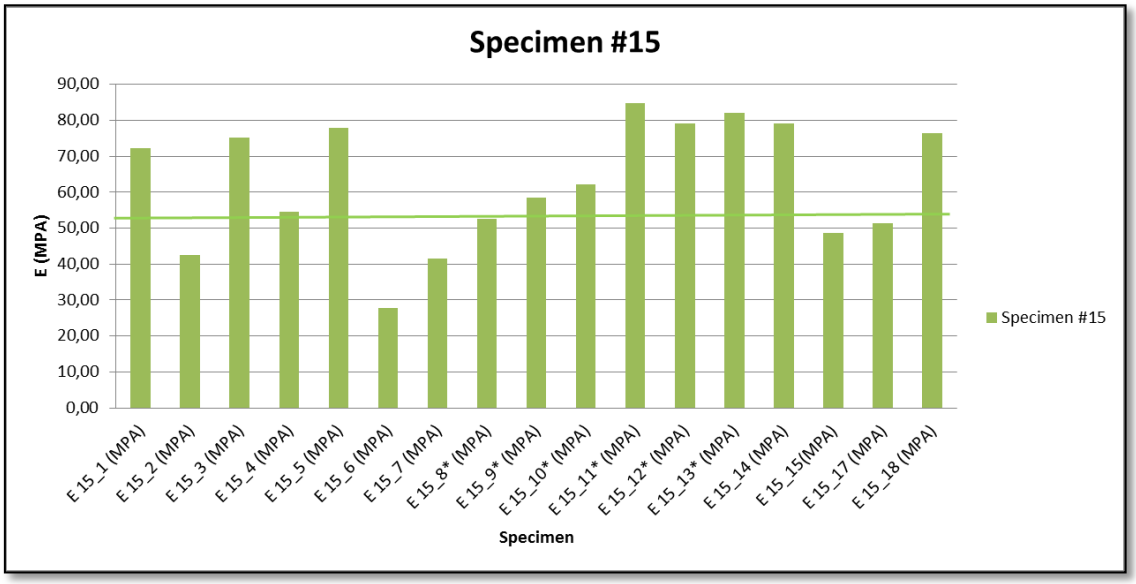

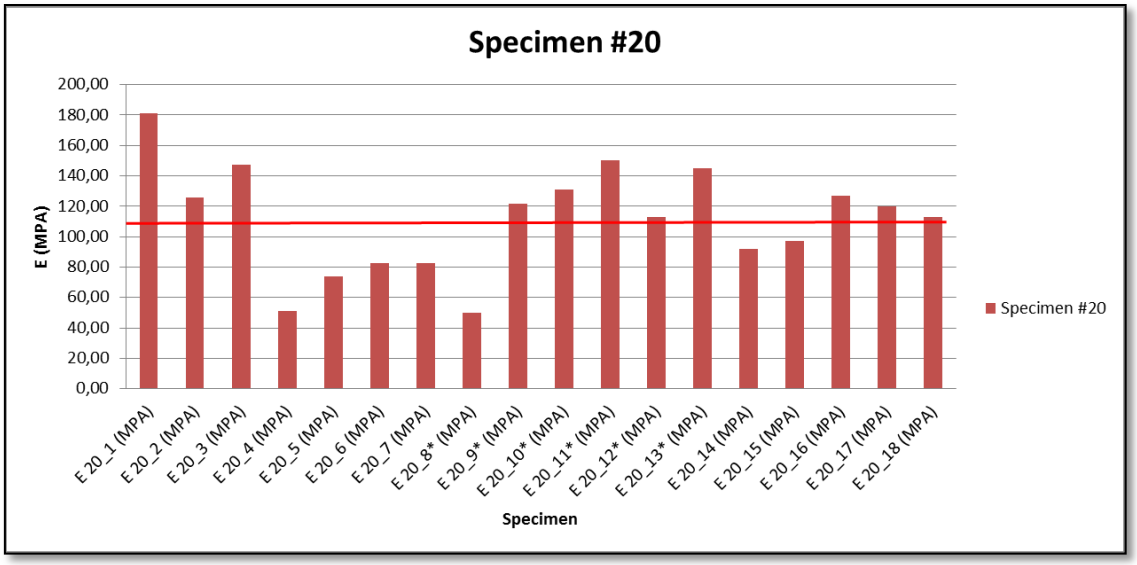
Specimen #20
200,00
180,00
160,00
140,00
120,00
100,00
80,00
60,00
40,00
20,00
0,00
E (MPA)
E 20_1 (MPA)
E 20_2 (MPA)
E 20_3 (MPA)
E 20_4 (MPA)
E 20_5 (MPA)
E 20_6 (MPA)
E 20_7 (MPA)
E 20_8* (MPA)
E 20_9* (MPA)
E 20_10* (MPA)
E 20_11* (MPA)
E 20_12* (MPA)
E 20_13* (MPA)
E 20_14 (MPA)
E 20_15 (MPA)
E 20_16 (MPA)
E 20_17 (MPA)
E 20_18 (MPA)
Specimen
Specimen #20

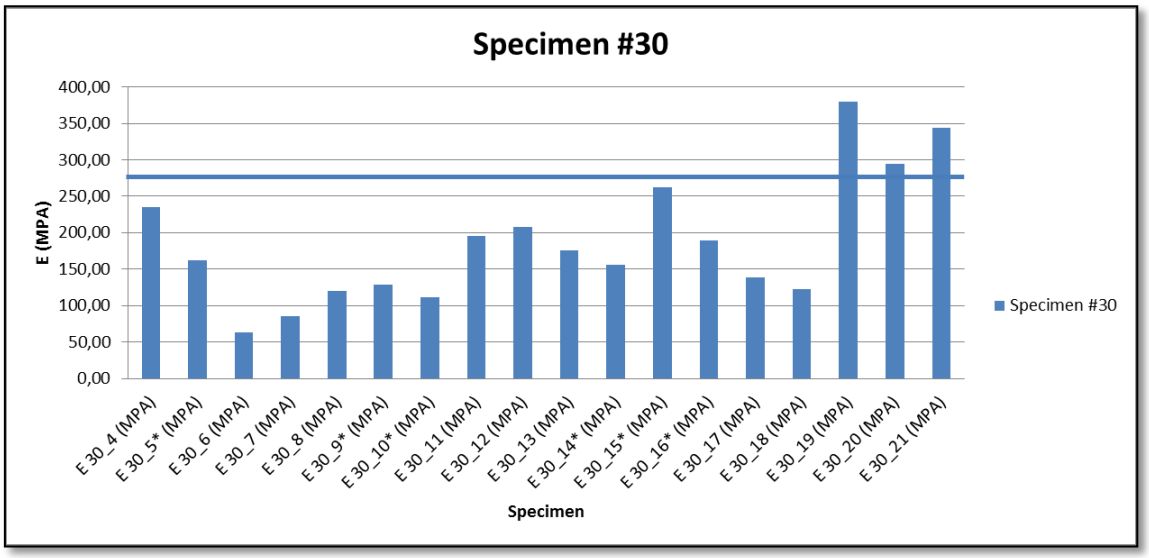
Specimen #30
400,00
350,00
300,00
250,00
200,00
150,00
100,00
50,00
0,00
E (MPA)
E 30_4 (MPA)
E 30_5* (MPA)
E 30_6 (MPA)
E 30_7 (MPA)
E 30_8 (MPA)
E 30_9* (MPA)
E 30_10* (MPA)
E 30_11 (MPA)
E 30_12 (MPA)
E 30_13 (MPA)
E 30_14* (MPA)
E 30_15* (MPA)
E 30_16* (MPA)
E 30_17 (MPA)
E 30_18 (MPA)
E 30_19 (MPA)
E 30_20 (MPA)
E 30_21 (MPA)
Specimen
Specimen #30